arXiv:1402.6542v1 [math.DS] 26 Feb 2014

Brownian dynamics of immersed bodies by a meshfree particle method for incompressible fluctuating hydrodynamics

Anamika Pandey[a,], Steffen Hardt[b], Axel Klar[a], Sudarshan Tiwari[a]

[a] *Fachbereich Mathematik, Technische Universität Kaiserslautern, Erwin-Schrödinger-Str. , 67663 Kaiserslautern, Germany*
[b] *Institute for Nano- and Microfluidics, Center of Smart Interfaces, Technische Universität Darmstadt, Alarich-Weiss-Str. 10, 64287 Darmstadt, Germany*

Abstract

A meshfree Lagrangian method for the fluctuating hydrodynamic equations (FHEs) with fluid-structure interactions is presented. Brownian motion of particles is investigated by direct numerical simulation of the fluctuating hydrodynamic equations. In this framework a bidirectional coupling has been introduced between the fluctuating fluid and the solid object. The force governing the motion of the solid object (Newton-Euler equations) is solely due to the surrounding fluid particles. Since a meshfree formulation is used, the method can be extended to many real applications involving complex fluid flows. Two and three-dimensional implementations along with qualitative and quantitative validations are presented. In particular, the Stokes-Einstein relation is reproduced.

Keywords:
Brownian dynamics, fluctuating hydrodynamics, meshfree method, stochastic partial differential equation, bidirectional coupling, fluctuation-dissipation theorem.

Email addresses: pandey@mathematik.uni-kl.de (Anamika Pandey), hardt@csi.tu-darmstadt.de (Steffen Hardt), klar@mathematik.uni-kl.de (Axel Klar), tiwari@mathematik.uni-kl.de (Sudarshan Tiwari)

1. Introduction

Recently, the flow of fluids in small scale geometries became technologically important, for example, in nanotechnology applications. In particular, the interaction of micro/nano scale objects with the fluid in such small scale geometries is an important topic. As one approaches smaller scales, thermal fluctuations play an essential role in the description of the fluid flow. These fluctuations need to be considered on different levels of description, see [1, 2, 3]. Thermodynamic fluctuations have been thoroughly studied at equilibrium as well as at non-equilibrium in many textbook of statistical mechanics such as [4, 5].

In fluid dynamics, thermal fluctuations are either included in continuum field models or described on a microscopic level using methods like molecular dynamics. If one concentrates on continuum field descriptions, fluctuations are included into partial differential equations via stochastic terms. The classical equations in that context are stochastic partial differential equations (SPDEs), where the divergence of a white noise process is added to the conventional Navier-Stokes equations. These equations have been termed as the Landau-Lifshitz Navier-Stokes (LLNS) equations and were first proposed in [6]. This approach models the thermal fluctuations via random stress terms in the momentum equation in the case of incompressible flow. The LLNS equations belong to the most complex examples in the broad family of SPDEs. Initially, the LLNS equations have been presented for fluctuations around an equilibrium state of a system, but later on their validity for non-equilibrium systems has been shown [7] and verified by molecular simulations [8, 9].

Early work in the context of numerical schemes for LLNS equations has been done by Garcia et al. [10]. The authors have developed a simple scheme for the stochastic heat conduction equation and the linearized one-dimensional LLNS equations. Later on in [11] a centered scheme based on a finite-volume method (FVM) combined with a third-order Runge-Kutta (RK3) scheme for the compressible LLNS equations has been introduced. Afterwards, a systematic approach for the analysis of grid based FVMs for the LLNS equations and related SPDEs has been discussed by Donev et al. [12], the extension of numerical solvers for the LLNS equations to binary mixtures in three dimensions and staggered schemes for fluctuating hydrodynamics have been presented in [13, 14]. A meshfree Lagrangian formulation for the 1D LLNS equations for compressible fluid has been presented by the present

authors [15] and the results have been compared to the well established FVM based RK3 scheme.

In the context of fluid-structure interactions, the Brownian motion of particles governed by fluctuating hydrodynamic equations has been investigated in [16]. There, inertia terms in the governing equations have been neglected and the resultant time independent problem has been solved with a numerical approach using a fixed grid. An immersed boundary approach has been reported by Atzberger [17] for fluid-structure interaction with thermal fluctuations using a grid based method.

The present work distinguishes itself from the existing literature in its approach as well as in additional validation cases. An explicit coupling strategy has been used between the fluctuating fluid and the solid structure, and a numerical algorithm based on a meshfree formulation is used for the LLNS equations. For the validation, 2D and 3D Brownian motions of particles are investigated and the Stokes-Einstein relation is tested.

Although a meshfree method termed "Smoothed dissipative particle dynamics (SDPD)" has been presented in [18] which incorporates thermal fluctuations, this is the first formulation of a meshfree method for solving the fluctuating hydrodynamic equations which is based on solving stochastic partial differential equations. The SDPD is a combination of meshfree smoothed particle hydrodynamics (SPH) [19] and dissipative particle dynamics (DPD) [20]. In this approach, the SPH discretization of the Navier-Stokes equations is performed and then thermal fluctuations are treated in the same way as in DPD. In the present meshfree method, the continuum constitutive model with stochastic stress tensor is considered, and then a numerical approximation for the stochastic partial differential equations is employed.

Meshfree methods are particularly suited for problems with time-varying fluid domains such as problems with bodies suspended in a fluid because a meshfree method eliminates the difficulties arising in a time-varying computational domain such as re-meshing and changing topology. This meshfree approach for the simulation of fluid-structure interactions is based on a Lagrangian formulation of the complete system which handles the fluid-structure interface in a smooth and efficient way.

2. Governing Equations

We consider a rigid sphere inside an incompressible fluctuating fluid. Let $\Omega \subset \mathbb{R}^d$ ($d = 2$ or 3) denote the entire computational domain including

both fluid and rigid body, the domain of the rigid body is denoted by P. A neutrally buoyant solid particle is considered.

The governing equations for the motion of the incompressible fluctuating fluid are given by

$$\rho_f \frac{d\mathbf{u}}{dt} = \nabla \cdot \boldsymbol{\sigma} \qquad \text{in } \Omega \setminus P, \tag{1}$$

$$\nabla \cdot \mathbf{u} = 0 \qquad \text{in } \Omega \setminus P, \tag{2}$$

where ρ_f denotes the density of the fluid. $\dfrac{d}{dt} = \dfrac{\partial}{\partial t} + \mathbf{u}.\nabla$ defines the material derivative. The stress $\boldsymbol{\sigma}$ is given by

$$\boldsymbol{\sigma} = -pI + \mu[\nabla\mathbf{u} + (\nabla\mathbf{u})^T] + \widetilde{\mathbf{S}}, \tag{3}$$

where p is the pressure and μ is the dynamic viscosity of the surrounding fluid. $\widetilde{\mathbf{S}}$ stands for the stochastic stress tensor, which models the inherent molecular fluctuations in the fluid. The required stochastic properties of $\widetilde{\mathbf{S}}$ have been derived by Landau and Lifshitz [6] in the spirit of a fluctuation-dissipation balance principle, described as

$$\langle \widetilde{S}_{ij}(\mathbf{x}, t) \rangle = 0, \tag{4a}$$

$$\langle \widetilde{S}_{ik}(\mathbf{x}, t) \widetilde{S}_{lm}(\mathbf{x}', t') \rangle = 2k_B T \mu (\delta_{il}\delta_{km} + \delta_{im}\delta_{kl}) \delta(\mathbf{x} - \mathbf{x}') \delta(t - t'), \tag{4b}$$

where k_B is the Boltzmann constant, T is the temperature of the fluid and $\langle\ \rangle$ is used for ensemble averages. It has to be noted that originally these expressions have been derived for compressible fluids, but equation (4) is the corresponding approximation for incompressible fluids.

The motion of the rigid sphere inside the incompressible fluctuating fluid is governed by the Newton-Euler equations

$$M \frac{d\mathbf{U}}{dt} = \mathbf{F}, \tag{5}$$

$$\mathbf{I} \frac{d\boldsymbol{\omega}}{dt} = \mathbf{T}. \tag{6}$$

Here, $\mathbf{U}$ and $\boldsymbol{\omega}$ represent the translational and rotational velocities of the solid, respectively. M and $\mathbf{I}$ denote mass and moment of inertia of the rigid body, respectively. $\mathbf{F}$ is the resultant hydrodynamic force acting on the rigid body from the surrounding fluid,

$$\mathbf{F} = (-1) \int_{\partial P} \boldsymbol{\sigma} \hat{\mathbf{n}}_s \, \mathrm{d}(\partial P). \tag{7}$$

$\mathbf{T}$ denotes the hydrodynamic torque of the hydrodynamical force on the rigid body

$$\mathbf{T} = (-1) \int_{\partial P} \mathbf{r} \times (\boldsymbol{\sigma} \hat{\mathbf{n}}_s) \, \mathrm{d}(\partial P), \tag{8}$$

where $\hat{\mathbf{n}}_s$ is the unit outward normal on the surface of the rigid body. $\mathbf{r} = \mathbf{x} - \mathbf{X}_{cm}$ is the position vector with respect to the center of mass ($\mathbf{X}_{cm}$) of the rigid body. The center of mass $\mathbf{X}_{cm}$ and the orientation Θ of the rigid body are updated by

$$\frac{d\mathbf{X}_{cm}}{dt} = \mathbf{U}, \tag{9}$$

$$\frac{d\Theta}{dt} = \boldsymbol{\omega}. \tag{10}$$

Together, equations (5 - 10) describe the motion of the rigid body.

This formulation has to be complemented by appropriate initial and boundary conditions for the fluid-structure system. Let us denote the outer boundary of the computational domain Ω, which is not shared by the rigid sphere, by Γ. We consider a simple cubic array of domains. Therefore periodic boundary conditions are employed on Γ, given as

$$\begin{aligned} \mathbf{u}_{\Gamma_L} &= \mathbf{u}_{\Gamma_R} \\ \frac{\partial \mathbf{u}}{\partial \mathbf{n}} \, |_{\Gamma_L} &= -\frac{\partial \mathbf{u}}{\partial \mathbf{n}} \, |_{\Gamma_R}, \end{aligned} \tag{11}$$

where $\mathbf{n}$ denotes the unit outward normal on Γ. Γ_L and Γ_R are the left and right faces of the boundary Γ. Since we have periodicity in all directions similar boundary conditions hold at the top - bottom and front - back faces.

The no-slip boundary condition is considered on ∂P which is the interior boundary of the fluid and the surface of the rigid body

$$\mathbf{u} = \mathbf{U} + \boldsymbol{\omega} \times \mathbf{r} = \mathbf{v} \qquad \text{on } \partial P. \tag{12}$$

$\mathbf{v}$ represents the resultant velocity of the rigid sphere, which also gives the flow velocity at the interface.

The initial condition for the fluid is defined as

$$\mathbf{u}(t = 0) = \mathbf{u}_0, \tag{13}$$

where $\mathbf{u}_0$ should satisfy equation (2). The initial conditions for the suspended particle are

$$\mathbf{X}_{cm}(t = 0) = \mathbf{X}_{cm0}; \quad \Theta(t = 0) = \Theta_0; \quad \mathbf{U}(t = 0) = \mathbf{U}_0; \quad \boldsymbol{\omega}(t = 0) = \boldsymbol{\omega}_0, \tag{14}$$

where $\mathbf{X}_{cm0}, \mathbf{U}_0, \boldsymbol{\omega}_0$ should satisfy equation (12) such that for the resultant velocity of the rigid body $\mathbf{v}_0 = \mathbf{u}_0$.

In this study, we have considered the incompressible LLNS equations for the fluctuating fluid and the Newton-Euler equations for the motion of the solid object without any external forces. Due to the consideration of a spherical particle made of homogeneous material, the non-linear term $\boldsymbol{\omega} \times \mathbf{I}\boldsymbol{\omega}$ vanishes in the equation (6).

3. Numerical Approximation

In this section, we will discuss the numerical approximation of the coupled system. It has to be noticed that the stochastic forcing in the LLNS equations is a divergence of a white noise process, rather than the more common external fluctuations modelled through white noise which have been discussed in [21, 22, 23]. The occurrence of the divergence operator in front of white noise makes the numerical approximation of the LLNS equations difficult. However, a systematic analysis of the numerical discretization of the LLNS equations in the context of finite-volume methods has been discussed in [12].

In the present work, a meshfree method is used for the spatial discretization. Spatially discretized points in the spatial domain are defined by material points, i.e. they move with the fluid velocity. These mesh particles carry all relevant physical properties of the fluid. For the time integration a projection based scheme for the fluid motion and an explicit Euler scheme for the motion of the rigid body have been used. We take a fixed time step Δt throughout the computation.

The spatio-temporal averaging of stochastic forcing is performed in the same way as explained in [12, 14]. The components of stochastic fluxes are generated as

$$\widetilde{\mathbf{S}} = \left(\widetilde{S}_{ij}\right) = \sqrt{\frac{2\mathcal{A}_{ij} k_B T \mu}{\Delta V \Delta t}} \widetilde{\mathfrak{R}}, \tag{15}$$

where $\mathcal{A}_{ij} = 2$, for $i = j$ and 1 otherwise. $\widetilde{\mathfrak{R}} = \dfrac{\mathfrak{R} + \mathfrak{R}^T}{2}$. A realization of $\widetilde{\mathfrak{R}}$ is sampled by an independent and identically distributed (iid) standard normal variable (a stream of normally distributed random numbers with mean zero and variance one) at each time step. $\Delta V = \dfrac{V}{N}$, where V is the volume of the fluid domain $\Omega \setminus P$ and N is the number of spatial discretized points at

a particular time step. In the meshfree formulation N does not remain fixed over time. Therefore, ΔV changes over time and has to be appropriately updated at each time step.

3.1. Time Integration

At first we explain the time discretization of the fluid equations and then the coupling of fluid and rigid body motion.

3.1.1. Time integration of the LLNS equations

For the fluctuating fluid dynamic equations, we have employed an extension of the Chorin projection scheme [24]. In the next subsection, the spatial discretization of the differential operators will be described. These discretized differential operators are denoted by letter symbols to distinguish them from the corresponding continuum operators. For example, $\mathbf{G}$ denotes the discretized gradient operator, $\mathbf{L}$ and $\mathbf{D}$ stand for the discretized Laplacian and divergence operators, respectively. A temporal discretization of the LLNS system has to reproduce the statistical properties of the continuum fluctuations, which is an additional challenge for the temporal scheme. We would like to mention that the temporal integration of fluctuating hydrodynamics can be higher order accurate only in the weak sense and only for linearized equations of fluctuating hydrodynamics [12].

We index the time step by a superscript n, i.e. quantities evaluated at time $n\Delta t$ are denoted by the superscript n.

Since we use a Lagrangian description of the fluid, an additional equation has to be solved for the trajectory of a material point together with equations (1 - 14). This equation also provides the moving mesh for spatial discretization and can be written as

$$\frac{d\mathbf{x}}{dt} = \mathbf{u}. \tag{16}$$

At the first step of the projection scheme, we compute the new positions of the mesh particles from equation (16) and the intermediate velocity $\mathbf{u}^*$ from equation (1) by ignoring the pressure term:

$$\mathbf{x}^{n+1} = \mathbf{x}^n + \Delta t \mathbf{u}^n, \tag{17}$$

$$\mathbf{u}^* = \mathbf{u}^n + \frac{\Delta t}{\rho_f}(\mu \mathbf{L}\mathbf{u}^n + \mathbf{D}\widetilde{\mathbf{S}}^n). \tag{18}$$

Then, we correct the intermediate velocity $\mathbf{u}^*$ by its projection onto the space of solenoidal velocity fields

$$\mathbf{u}^{n+1} = \mathbf{u}^* - \frac{\Delta t}{\rho_f}\mathbf{G}p^{n+1}. \tag{19}$$

This requires the gradient of the pressure field at the $(n+1)^{th}$ time step. For this a pressure Poisson equation is solved which comes from the incompressibility condition. Since

$$\mathbf{D}\mathbf{u}^{n+1} = 0, \tag{20}$$

this gives

$$\mathbf{L}p^{n+1} = \frac{\rho_f}{\Delta t}\mathbf{D}\mathbf{u}^*. \tag{21}$$

The boundary condition for the pressure p is obtained by the projection of equation (19) onto the normal $\mathbf{n}$ of the boundary $\partial\Omega(= \Gamma \cup \partial P)$. Thus we will get a Neumann boundary condition for pressure, which is given as

$$\left(\mathbf{G}p^{n+1} \cdot \hat{\mathbf{n}}\right)|_{\partial\Omega} = -\frac{\rho_f}{\Delta t}(\mathbf{u}^{\mathbf{n+1}}_{\partial\mathbf{\Omega}} - \mathbf{u}^*_{\partial\mathbf{\Omega}}) \cdot \hat{\mathbf{n}}. \tag{22}$$

By noting that $\mathbf{u}^*|_{\partial\Omega} = \mathbf{u}^{n+1}_{\partial\Omega}$ and $\mathbf{n} \cdot \mathbf{u}^{n+1}|_{\partial\Omega} = \mathbf{n} \cdot \mathbf{u}^{n+1}_{\partial\Omega}$

$$\left(\mathbf{G}p^{n+1} \cdot \hat{\mathbf{n}}\right)|_{\partial\Omega} = 0. \tag{23}$$

Therefore, the velocity $\mathbf{u}^{n+1}$ is only guaranteed to satisfy the normal component of the boundary condition. However, since $\mathbf{u}^*$ does satisfy the full condition, it is expected that the error in the tangential component will be small.

In this scheme, we update the positions of mesh particles only once, and then the intermediate velocity, the final divergence free velocity field and the pressure field are computed at these new particle positions. The stochastic flux $\widetilde{\mathbf{S}}$ is updated at each time step as described earlier.

3.1.2. Time integration for the solid structure

For the fluid-structure interaction we have to couple the Newton-Euler equations for the solid motion given by equations (5 - 10) with the LLNS equations. We use an explicit method for the time discretization of the Newton-Euler equations. The main steps are as follows

1. Once we get the value of $\mathbf{u}^{n+1}$, p^{n+1} and the value of $\widetilde{\mathbf{S}}^{n+1}$ (based on the stream of pseudo-random numbers) compute the stress $\boldsymbol{\sigma}^{n+1}$ according to equation (3)

$$\boldsymbol{\sigma}^{n+1} = -p^{n+1}I + \mu[\nabla \mathbf{u}^{n+1} + (\nabla \mathbf{u}^{n+1})^T] + \widetilde{\mathbf{S}}^{n+1}. \tag{24}$$

2. Compute the hydrodynamic force and torque by a numerical approximation of the surface integrals, given by equations (7) and (8). To simulate the hydrodynamic interactions between the fluctuating fluid and the solid body, the solid body is defined by a boundary surface. In the numerical computation, this boundary surface is constructed by many point-like particles. The numerical approximation of the solid sphere is illustrated in figure 1. Thus, the components of the hydrodynamic force and the torque are computed as

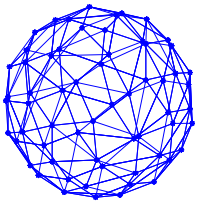

Figure 1: Location of boundary nodes to construct the boundary surface of sphere.

$$F_i = -\sum_{\mathbf{x}\in\partial P} \left((\boldsymbol{\sigma}\cdot\hat{\mathbf{n}}_\mathbf{s})_i\right)_\mathbf{x} ds_\mathbf{x}, \tag{25}$$

$$T_i = -\sum_{\mathbf{x}\in\partial P} \left(((\mathbf{x}-\mathbf{X}_\mathbf{cm})\times(\boldsymbol{\sigma}\cdot\hat{\mathbf{n}}_\mathbf{s}))_i\right)_\mathbf{x} ds_\mathbf{x}, \tag{26}$$

where i runs from 1 to 3, and $ds_\mathbf{x}$ is the area of the small surface element. In a $3D$ numerical simulation, this small surface element is a triangle which is formed by three closest nodes on the boundary surface. For a $2D$ simulation, where the rigid body is a circular disk, $ds_\mathbf{x}$ is the length of small line element, on the circumference of the disk.

3. Solve the equations of motion for the solid structure given by equations (5, 6, 9 and 10) together with given initial conditions:

$$\mathbf{X}_{cm}^{n+1} = \mathbf{X}_{cm}^{n} + \Delta t \mathbf{U}^{n}, \tag{27}$$

$$\Theta^{n+1} = \Theta^{n} + \Delta t \boldsymbol{\omega}^{n}, \tag{28}$$

$$\mathbf{U}^{n+1} = \mathbf{U}^{n} + \frac{\Delta t}{M} \mathbf{F}^{n}, \tag{29}$$

$$\boldsymbol{\omega}^{n+1} = \boldsymbol{\omega}^{n} + \Delta t \mathbf{I}^{-\mathbf{1}} T. \tag{30}$$

4. Compute the resultant velocity of the structure which will yield the interface boundary condition for the fluid flow

$$\mathbf{v}^{n+1} = \mathbf{u}^{n+1} = \mathbf{U}^{n+1} + \boldsymbol{\omega}^{n+1} \times (\mathbf{x} - \mathbf{X}_{cm}^{n+1}). \tag{31}$$

5. Move the boundary surface nodes of rigid body as described in step (2), with the resultant velocity $\mathbf{v}^{n+1}$

$$\mathbf{x}^{n+1} = \mathbf{x}^{n} + \Delta t \mathbf{v}^{n+1}. \tag{32}$$

We note that instead of the simple explicit first order time discretization used here, one could use a higher order scheme. It has to be noted that an explicit discretization of the Newton-Euler equations in the coupling of fluid-structure interaction works for the situation considered here, see the second point discussed below.

As it has been mentioned in [25], there are mainly two difficulties appearing in the fluid-structure simulation by explicit coupling.

1. **Regeneration of mesh:** The main approaches to handle re-meshing in the existing literature are as follows: Independent new mesh generation and the projection of the relevant information onto the new mesh from the old mesh [25], Arbitrary Lagrangian-Eulerian (ALE) mesh movement [26] and the fictitious domain approach [27].

   The task of mesh regeneration can be easily handled in the present meshfree formulation since we are working with a Lagrangian description of the fluid. The material points will move with the velocity of the fluid and the solid-fluid interface is accurately recaptured. Therefore, the computational domain is appropriately transformed in each time step.

2. **Explicit discretization of the Newton-Euler equations:** It has been mentioned in [25] that a fully explicit scheme for fluid-structure simulation will be unstable in certain situations due to the explicit discretization of the equations of translational motion of the solid particle. In [25] a condition for stability of the explicit scheme has been derived as $M_v < M$, where M_v denotes the so-called virtual mass of the fluid.

   Now, in the case of a spherical object, the virtual mass in an infinite fluid medium is given by

$$M_v = \frac{2}{3}\pi r^3 \rho_f, \tag{33}$$

   and the actual mass of the sphere is

$$M = \frac{4}{3}\pi r^3 \rho_s. \tag{34}$$

   Hence, $M_v < M$ if $\rho_f < 2\rho_s$.

   We have strictly followed this condition in our simulation by considering a neutrally buoyant spherical particle.

This completes the temporal discretization of the fluid-structure system. The remaining task is to approximate the spatial derivatives.

3.2. Spatial discretization

An algorithm for the meshfree solution of the incompressible Navier-Stokes equations has been presented in [28].

Let $f : \Omega \times [0, T] \longrightarrow \mathbb{R}$ be a scalar-valued function. $f(\mathbf{x}, t)$ denotes the value of the function f at position $\mathbf{x} \in \Omega$ at an instant t. In this formulation, the spatial differential operators acting on f are approximated at $\mathbf{x}$ in terms of the values of the function $f(\mathbf{x}, t)$ at a set of neighbouring points of $\mathbf{x}$. We define a weight function $w = w(\mathbf{x}_j - \mathbf{x}, h)$ with compact support h to have a limitation on the neighbouring points of $\mathbf{x}$. The choice of the weight function can be arbitrary. We choose a Gaussian weight function

$$w\left(\mathbf{x}_j - \mathbf{x}; h\right) = \begin{cases} \exp\left(-\alpha \dfrac{\|\mathbf{x}_j - \mathbf{x}\|^2}{h^2}\right), & \text{if } \dfrac{\|\mathbf{x}_j - \mathbf{x}\|}{h} \leq 1 \\ 0, & \text{else.} \end{cases} \tag{35}$$

where α is a positive constant and h defines the neighbourhood radius for $\mathbf{x}$. There is some obvious restriction on the location of the neighbouring

particles of $\mathbf{x}$ concerning the distribution and the number of particles in the neighbourhood. Then, the Taylor expansion of $f(\mathbf{x}, t)$ around $\mathbf{x} = (x, y, z)$ yields a linear system in the unknown derivatives, reading

$$\mathbf{e} = M\mathbf{a} - \mathbf{b}. \tag{36}$$

If $\mathbf{x}$ has m neighbours, at an instant, then

$$M = \begin{bmatrix} \Delta x_1 & \Delta y_1 & \Delta z_1 & \frac{\Delta x_1^2}{2} & \Delta x_1 \Delta y_1 & \Delta x_1 \Delta z_1 & \frac{\Delta y_1^2}{2} & \Delta y_1 \Delta z_1 & \frac{\Delta z_1^2}{2} \\ \Delta x_2 & \Delta y_2 & \Delta z_2 & \frac{\Delta x_2^2}{2} & \Delta x_2 \Delta y_2 & \Delta x_2 \Delta z_2 & \frac{\Delta y_2^2}{2} & \Delta y_2 \Delta z_2 & \frac{\Delta z_2^2}{2} \\ \vdots & \vdots & \vdots & \vdots & \vdots & \vdots & \vdots & \vdots & \vdots \\ \Delta x_m & \Delta y_m & \Delta z_m & \frac{\Delta x_m^2}{2} & \Delta x_m \Delta y_m & \Delta x_m \Delta z_m & \frac{\Delta y_m^2}{2} & \Delta y_m \Delta z_m & \frac{\Delta z_m^2}{2} \end{bmatrix},$$

$$\mathbf{a} = [f^x \quad f^y \quad f^z \quad f^{xx} \quad f^{xy} \quad f^{xz} \quad f^{yy} \quad f^{yz} \quad f^{zz}]^T,$$

$$\mathbf{b} = [f_1 - f \quad f_2 - f \quad \dots \quad \dots \quad \dots \quad f_m - f]^T,$$

$$\mathbf{e} = [e_1 \quad e_2 \quad \dots \quad \dots \quad \dots \quad e_m]^T.$$

Here, $\Delta x_i = x_i - x$, $\Delta y_i = y_i - y$, $\Delta z_i = z_i - z$ for $i = 1, \dots m$, and superscript x, y, z on f represent the respective partial derivatives of function.

This system is solved using a least square approximation by minimizing,

$$J = \sum_{i=1}^{m} w_i e_i^2 = (M\mathbf{a} - \mathbf{b})^T W (M\mathbf{a} - \mathbf{b}), \tag{37}$$

where $W = diag[w_1 \dots w_n]$ is a diagonal matrix, whose entries $w_i = w(\mathbf{x}_i - \mathbf{x}; h)$ as given in equation (35).

This yields the unknown $\mathbf{a}$, as

$$\mathbf{a} = \left(M^T W M\right)^{-1} \left(M^T W\right) \mathbf{b}. \tag{38}$$

As a result, we will get derivatives of the prescribed function at a specific point as a linear combination of function values at its neighbour points.

In the present work, this approach will be also employed for the solution of the pressure Poisson equation with Neumann boundary conditions and for

periodic boundary conditions of the velocity. In general, these equations can be written in the following form

$$Af + B(\nabla f \cdot \mathbf{n}) + C(\nabla^2 f) = g, \tag{39}$$

where A, B and C are real constants and g is a known real valued function. All equations appearing in the process of Chorin's projection can be derived from equation (39) for different choices of A, B, C and g. For example, in the pressure Poisson equation (21)

$$A = 0, B = 0, C = 1 \text{ and } g = \frac{\rho_f}{\Delta t}\nabla \cdot \mathbf{u}^*. \tag{40}$$

This approach was first presented in [29] to solve the Poisson equation. The accuracy and stability of this method to solve the pressure Poisson equation with different boundary conditions is also discussed by [29].

Let us consider that we have to solve equation (39) together with a Robin boundary condition

$$b_1 f + b_2 \nabla f \cdot \hat{\mathbf{n}} = h. \tag{41}$$

As discussed above, we will again consider the set of neighbouring points for a given point $\mathbf{x}$ to compute the derivatives of a function and its value. Unlike the previous case, the value of the function is also unknown. We will incorporate the equations (39) and (41) with appropriate constants and functions into the least square approximation as additional constraints for each mesh point $\mathbf{x}$. For any interior point of the domain, b_1 and b_2 will be zero in equation (41). Again, the Taylor series expansion of f is performed but due to the unknown function values the considered system $\mathbf{e} = M\mathbf{a} - \mathbf{b}$ is defined by

$$M = \begin{bmatrix} 1 & \Delta x_1 & \Delta y_1 & \Delta z_1 & \frac{\Delta x_1^2}{2} & \Delta x_1 \Delta y_1 & \Delta x_1 \Delta z_1 & \frac{\Delta y_1^2}{2} & \Delta y_1 \Delta z_1 & \frac{\Delta z_1^2}{2} \\ 1 & \Delta x_2 & \Delta y_2 & \Delta z_2 & \frac{\Delta x_2^2}{2} & \Delta x_2 \Delta y_2 & \Delta x_2 \Delta z_2 & \frac{\Delta y_2^2}{2} & \Delta y_2 \Delta z_2 & \frac{\Delta z_2^2}{2} \\ \vdots & \vdots & \vdots & \vdots & \vdots & \vdots & \vdots & \vdots & \vdots & \vdots \\ 1 & \Delta x_m & \Delta y_m & \Delta z_m & \frac{\Delta x_m^2}{2} & \Delta x_m \Delta y_m & \Delta x_m \Delta z_m & \frac{\Delta y_m^2}{2} & \Delta y_m \Delta z_m & \frac{\Delta z_m^2}{2} \\ A & Bn_x & Bn_y & Bn_z & C & 0 & 0 & C & 0 & C \\ b_1 & b_2 n_x & b_2 n_y & b_2 n_z & 0 & 0 & 0 & 0 & 0 & 0 \end{bmatrix}.$$

Here, n_x, n_y and n_z denote x, y and z components of the unit normal $\mathbf{n}$, respectively.

$$\begin{aligned}\mathbf{a} = \; & [f \quad f^x \quad f^y \quad f^z \quad f^{xx} \quad f^{xy} \quad f^{xz} \quad f^{yy} \quad f^{yz} \quad f^{zz}]^T, \\ \mathbf{b} = \; & [f_1 \quad f_2 \quad \dots \quad \dots \quad \dots \quad f_m \quad g \quad h]^T, \\ \mathbf{e} = \; & [e_1 \quad e_2 \quad \dots \quad \dots \quad \dots \quad e_m \quad e_{m+1} \quad e_{m+2}]^T.\end{aligned}$$

Now, the objective function J is

$$J = \sum_{i=1}^{m+2} w_i e_i^2 = (M\mathbf{a} - \mathbf{b})^T W (M\mathbf{a} - \mathbf{b}), \tag{42}$$

where $W = diag(w_1, \dots, w_m, 1, 1)$ with the same $w_i = w(\mathbf{x}_i - \mathbf{x}; h)$. The minimizer of J is

$$\mathbf{a} = \left(M^T W M\right)^{-1} \left(M^T W\right) \mathbf{b}. \tag{43}$$

Let us suppose that the first row of $\left(M^T W M\right)^{-1}$ is $\alpha = (\alpha_1, \dots, \alpha_{10})$. The explicit structure of $(M^T W)b$ is

$$(M^T W)b = \begin{bmatrix} \sum w_i f_i + Ag + b_1 h \\ \sum w_i \Delta x_i f_i + Bn_x g + b_2 n_x h \\ \sum w_i \Delta y_i f_i + Bn_y g + b_2 n_y h \\ \sum w_i \Delta z_i f_i + Bn_z g + b_2 n_z h \\ \sum w_i \frac{\Delta x_i^2}{2} f_i + Cg \\ \sum w_i \Delta x_i y_i f_i \\ \sum w_i \Delta x_i z_i f_i \\ \sum w_i \frac{\Delta y_i^2}{2} f_i + Cg \\ \sum w_i \Delta y_i z_i f_i \\ \sum w_i \frac{\Delta z_i^2}{2} f_i + Cg \end{bmatrix}.$$

For the first element of $\mathbf{a}$ these two pieces of information will be sufficient

and we can write

$$
\begin{aligned}
f - \sum_{i=1}^{m} w_i(\alpha_1 + \alpha_2\Delta x_i + \alpha_3\Delta y_i + \alpha_4\Delta z_i + \alpha_5\frac{\Delta x_i^2}{2} + \alpha_6\Delta x_i\Delta y_i \\
+ \alpha_7\Delta x_i\Delta z_i + \alpha_8\frac{\Delta y_i^2}{2} + \alpha_9\Delta y_i\Delta z_i + \alpha_{10}\frac{\Delta z_i^2}{2})f_i \\
= (\alpha_1 A + \alpha_2 Bn_x + \alpha_3 Bn_y + \alpha_4 Bn_z + \alpha_5 C + \alpha_8 C + \alpha_{10} C)g \\
+ (\alpha_1 b_1 + \alpha_2 b_2 n_x + \alpha_3 b_2 n_y + \alpha_4 b_2 n_z)h. \qquad (44)
\end{aligned}
$$

Note that f is the value of function at the considered point x and f_i for $i = 1, \ldots, m$ is the values of function at the neighbours of x, and they all are unknown. By repeating this procedure for all interior and boundary particles we get a linear system for the unknowns f_j for $j = 1, \ldots, N$, where N is the total number of particles in the domain. It has to be mentioned that when considering a particle $\mathbf{x}$ the only non-zero coefficients appearing in equation (44) are for the particle itself and its neighbours. Therefore the resultant linear system will be very sparse for large N. This sparse linear system can be solved by any standard iterative method. We have used the Gauss-Seidel method. For the initial guess in an iteration step we will use the value of the previous time step. On getting the function values we can compute the required derivatives as described earlier.

4. Numerical results

In this section we present our simulation results. In the first part we discuss the results for a two-dimensional fluctuating fluid and investigate the Brownian motion of a solid disc. In the second part, we investigate three-dimensional Brownian motion of a solid sphere due to fluctuating hydrodynamics and validate the Stokes-Einstein relation.

To proceed, the governing equations are non-dimensionalized. The fundamental scales for non-dimensionalization are chosen as

$$
\left.
\begin{aligned}
&\text{Characteristic length} \longrightarrow L = \text{System length}, \\
&\text{Characteristic time} \longrightarrow \widetilde{t} = \sqrt{\frac{\mu V \Delta t}{k_B T}}, \\
&\text{Characteristic mass} \longrightarrow \widetilde{M} = L\sqrt{\frac{\mu^3 V \Delta t}{k_B T}},
\end{aligned}
\right\} \qquad (45)
$$

here the system length L means the size of computational domain.

The resultant scaling for velocity, pressure and stress are

$$\left.\begin{aligned} &\text{Characteristic velocity} \longrightarrow \widetilde{v} = \frac{L}{\widetilde{t}} = L\sqrt{\frac{k_B T}{\mu V \Delta t}}, \\ &\text{Characteristic pressure, stress} \longrightarrow \widetilde{P}, \widetilde{S} = \sqrt{\frac{\mu k_B T}{V \Delta t}}. \end{aligned}\right\} \tag{46}$$

The resulting non-dimensionalized system of differential equations is

$$\frac{D\mathbf{u}^*}{Dt^*} = \frac{1}{Re_f}\left(-\nabla p^* + \triangle \mathbf{u}^* + \nabla \cdot \widetilde{\mathbf{S}}^*\right) \qquad \text{in} \quad \Omega \setminus P, \tag{47}$$

$$\nabla \cdot \mathbf{u}^* = 0 \qquad \text{in} \quad \Omega \setminus P, \tag{48}$$

$$\frac{d\mathbf{x}^*}{dt^*} = \mathbf{u}^* \qquad \text{in} \quad \Omega \setminus P, \tag{49}$$

$$\frac{d\mathbf{U}^*}{dt^*} = \frac{1}{Re_s}\frac{L^3}{V_s}\mathbf{F}^* \qquad \text{in} \quad P, \tag{50}$$

$$\mathbf{I}^*\frac{d\boldsymbol{\omega}^*}{dt^*} = \frac{1}{Re_s}T^* \qquad \text{in} \quad P, \tag{51}$$

$$\frac{d\mathbf{X}^*{}_{cm}}{dt^*} = \mathbf{U}^*, \tag{52}$$

$$\frac{d\Theta^*}{dt^*} = \boldsymbol{\omega}^*, \tag{53}$$

here, $Re_f = \dfrac{\rho_f \tilde{\mathbf{v}} L}{\mu}$ and $Re_s = \dfrac{\rho_s \tilde{\mathbf{v}} L}{\mu}$ are Reynold numbers formed with fluid and solid density, respectively. V_s denotes the volume of the solid. Non-dimensionalized variables are denoted by the superscript $*$.

The components of non-dimensionalized stochastic fluxes are given as

$$\widetilde{\mathbf{S}}^* = \left(\widetilde{S}^*_{ij}\right) = \sqrt{2N\mathcal{A}_{ij}}\widetilde{\mathfrak{R}}, \tag{54}$$

where N is the total number of material points in the spatial discretization of domain at an instant. A_{ij} and $\mathfrak{R}$ are same, as given for equation (15). $\mathbf{F}^*$ and $\mathbf{T}^*$ are given by

$$\mathbf{F}^* = (-1)\int_{(\partial P)} \boldsymbol{\sigma}^* \cdot \hat{\mathbf{n}}_s \, \mathrm{d}s^*, \tag{55}$$

$$\mathbf{T}^* = (-1)\int_{(\partial P)} \mathbf{r}^* \times (\boldsymbol{\sigma}^* \cdot \hat{\mathbf{n}}_s) \, \mathrm{d}s^*. \tag{56}$$

4.1. Brownian motion of a circular solid object in a two-dimensional fluctuating fluid

We consider a two-dimensional fluctuating fluid with an immersed circular solid object, initially placed at the center of the computational domain. We investigate the motion of the solid due to thermal fluctuations in the fluid. Neither in the solid domain nor in the fluid domain a body force is applied. The only forces responsible for the motion of the rigid body are the random stresses in the equations of motion of the fluid.

We consider a very small Reynolds number ($Re \ll 1$) and a neutrally buoyant particle, i.e. $\rho_f = \rho_s$. This implies $Re_f = Re_s = Re$. Initially, the fluid-structure system is at rest, i.e. $\mathbf{u_0}^* = 0$, $\mathbf{U_0}^* = 0$, and $\boldsymbol{\omega}_0^* = 0$. The random stresses are generated by iid Gaussian random numbers as given by equation (54). Once the random stresses are known, we solve the system of equations (47) - (53) by the described algorithm. We consider periodicity in all directions for the outer boundary Γ of the system and the no-slip boundary condition at the interface boundary ∂P.

We reproduce the characteristics of the Brownian motion of a circle in a two-dimensional fluctuating fluid to validate our numerical simulation. In figure 2, the trajectory of the center of mass (COM) of the disc from a specific simulation is shown. Figure 3 shows the PDF of the x-components of the

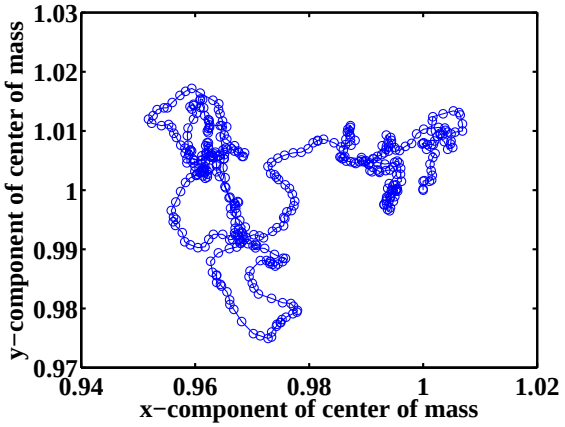

Figure 2: Trajectory of the center of mass of the disc.

relative linear velocity of the disc. It can be seen from the PDF in figure 3 that it fits very well to a Gaussian distribution.

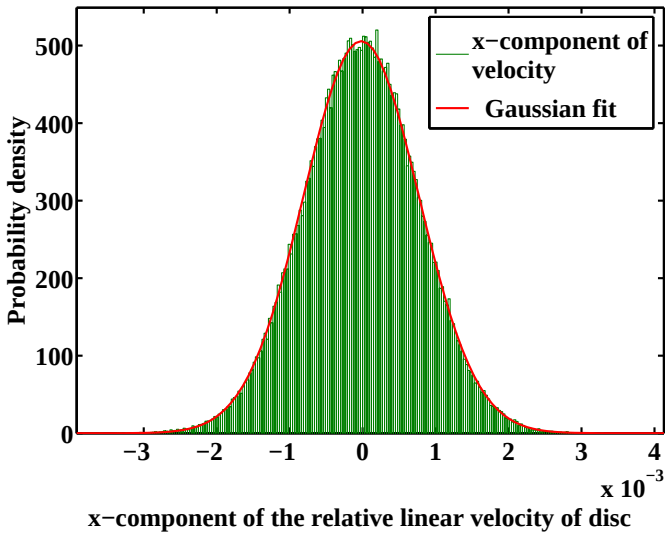

Figure 3: Comparison of the PDF of the x-velocity components with a Gaussian fit.

Within the numerical accuracy limits, the PDFs of both velocity components are identical, this reflects the isotropic property of Brownian motion. These observations draw a qualitative picture of the Brownian motion of a rigid disc. On a quantitative level, this case is less straightforward to analyze, as discussed in the following.

In the two-dimensional case, the usual Stokes-Einstein relation can not be formulated due to the Stokes' paradox. This inconsistency of the Stokes-Einstein relation in two dimensions has been discussed for example, in [30]. Nevertheless, research has been carried out to develop Stokes-Einstein type relations to relate various transport coefficients with sufficient accuracy. In this context, an important result is given in [31], relating the self-diffusion coefficient D of particles of a pure liquid to the viscosity coefficient of the liquid. For a pure liquid system, they proposed that $D\eta \propto T$, if one supplies appropriate redefinitions of the diffusion constant and viscosity coefficient.

Later on, in [32] a study of the transport coefficients in a hard disk system is presented. They considered a pure fluid composed of a large number of interacting hard discs. A test of the Stokes-Einstein relation was presented in [33], [34] for a two-dimensional fluid. In [33] a Stokes-Einstein type of relation

for a two-dimensional Yukawa liquid has been tested. They obtained

$$D = \frac{k_B T}{c_{2D} \eta \pi}. \tag{57}$$

The value of c_{2D} was found empirically to be 1.69 by a linear scaling of $D\eta$ with $k_B T$. The major difference between equation (57) and the usual Stokes-Einstein relation for three dimensions is the absence of the particle radius R in the denominator. In [34] this relation for the pure liquid case, i.e. a system of hard disks, has been reformulated in terms of the pair correlation function. Their results agree with the value of c_{2D} to be 1.69, at least for fluid density ranges as considered in the present work.

Owing to these difficulties and inspired by the findings for pure fluid systems, we now discuss the numerical results obtained for a fluctuating two-dimensional liquid without solid. We consider only the fluid system without the solid object and discuss a Stokes-Einstein type of relation to relate the self-diffusion coefficient of a tagged fluid particle to the viscosity of the fluid. For this case we use homogeneous Dirichlet boundary condition for the velocity.

It has to be noted that under the considered assumptions on the fluid system, the fluid flow occurs in the Stokes flow regime. Therefore, the velocity has to be interpreted in the same way as explained in [16]. Based on this interpretation, and for the chosen system in which no convective transport occurs, the fluid velocity $\mathbf{u}$ in equation (1) is due to the displacement of material volumes via Brownian diffusion once the dependencies on the initial condition is eliminated.

Therefore, the diffusion coefficient can be described as

$$D = \frac{\langle |\mathbf{u}(\Delta t)|^2 \rangle \Delta t}{4}, \tag{58}$$

where $\langle |\mathbf{u}(\Delta t)|^2 \rangle$ denotes the variance of the fluid velocity and is computed

as

$$\langle \mathbf{u} \rangle = \frac{1}{\sum_{n=1}^{N_s} M(n)} \left(\sum_{n=1}^{N_s} \sum_{i=1}^{M(n)} \mathbf{u}_i^n \right), \tag{59}$$

$$\langle |\mathbf{u}|^2 \rangle = \frac{1}{\sum_{n=1}^{N_s} M(n)} \left(\sum_{n=1}^{N_s} \sum_{i=1}^{M(n)} (\mathbf{u}_i^n)^2 \right) - \left(\frac{1}{\sum_{n=1}^{N_s} M(n)} \left(\sum_{n=1}^{N_s} \sum_{i=1}^{M(n)} \mathbf{u}_i^n \right) \right)^2, \tag{60}$$

where N_s is the total number of realizations and $M(n)$ is the total number of particles at time $n\Delta t$. Note that in the present computation ensemble averaging is equivalent to time averaging, due to the ergodicity of the system. This means that different trajectories of the tagged particle and the corresponding velocity for different realizations can be generated from the same simulation runs by considering different initial times at each time step. This means that going from $t \to t + \Delta t$ gives one realization by considering the initial time t, going from $t + \Delta t \to t + 2\Delta t$ gives another realization with initial time $t + \Delta t$. In the beginning, a number of initial time steps have been skipped to eliminate dependencies on the initial condition.

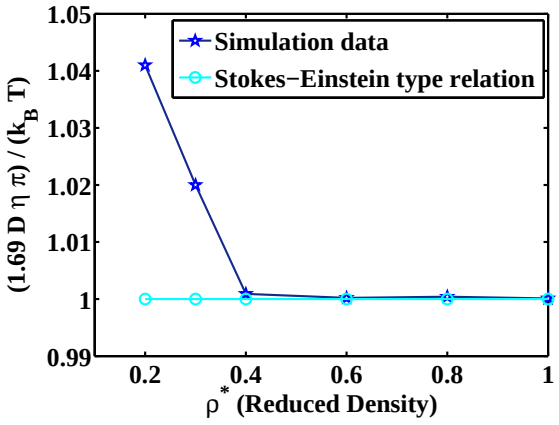

Figure 4: Verification of the Stokes-Einstein relation for two-dimensional fluids for different values of the density.

In figure, 4, we compare the numerical results to the Stokes-Einstein type relation for different densities. Our numerical results agree well with equation (57) for not too small densities. One can observe a discrepancy between the simulation data and equation (57) for smaller densities. But this discrepancy can be explained by the result in [34]. They have corrected equation (57) by a factor called the contact pair correlation function, which can be computed by molecular dynamics (MD) simulations. In the present work, we have not included this factor, but for the considered densities the simulation data in figure 4 show a similar trend as the results obtained in [34].

4.2. Brownian motion of a sphere in a three dimensional fluctuating fluid

In this subsection, we consider a sphere initially in the center of a cubic domain with periodic boundary conditions in all directions on the outer boundary Γ and no-slip boundary condition on interface boundary ∂P. No additional force is applied other than the stochastic force. The only forces responsible for the motion of the sphere are the random stresses. A neutrally buoyant spherical object immersed in an incompressible fluid with a very small Reynold number is considered. Initially, the fluid-structure system is at rest. Now, we solve the system of equations (47) - (53) for the three-dimensional fluid-structure system.

Under the above assumption, the fluid velocity $\mathbf{u}$ in equation (1) will be understood similar to the two-dimensional fluid system. Therefore, the linear and angular velocity of sphere must be interpreted in the same way.

Hence, the Brownian diffusion coefficient D of the sphere can be expressed as

$$D = \frac{\langle |\mathbf{U}_r(\Delta t)|^2 \rangle \Delta t}{2d}, \tag{61}$$

where d denotes the dimension of the space in which Brownian motion is considered. $\mathbf{U}_r$ is the relative velocity of the sphere with respect to the surrounding fluid.

On the other hand, for the free diffusion of a single particle in a fluid, the diffusion coefficient D is given by the Einstein's relation

$$D = \frac{k_B T}{\xi}, \tag{62}$$

where $k_B T$ is the thermal energy and ξ is the drag coefficient of the particle. For an isolated spherical particle of radius R in an infinite Newtonian fluid

with viscosity μ the Stokes drag $\mathbf{F}_S$ for translational motion is given by

$$\mathbf{F}_S = 6\pi\mu R\mathbf{U}_r, \tag{63}$$

where the Stokes drag coefficient is

$$\xi = 6\pi\mu R. \tag{64}$$

When a cubic domain with periodicity in all directions is considered, the drag coefficient is modified. The corresponding correction factor is defined as

$$\xi_c = \frac{|\mathbf{F}|}{|\mathbf{F}_S|}, \tag{65}$$

where $|\mathbf{F}|$ is the magnitude of the actual drag force (for a given relative velocity) on a solid sphere. The actual drag is equal to the Stokes drag for $\xi_c = 1$.

As a result, the actual diffusion constant D can be expressed as

$$D = \frac{k_B T}{6\pi\mu R\xi_c}. \tag{66}$$

The correction factor ξ_c appears due to the fact that for periodic boundary conditions there is an interaction between spheres belonging to the different copies of the computational domain. Equations (61) and (66) give us

$$\xi_c = \frac{6k_B T}{6\pi\mu R\Delta t\langle|\mathbf{U_r}(\Delta t)|^2\rangle}, \tag{67}$$

which reduces to

$$\xi_c = \frac{1}{\pi R^*\langle|\mathbf{U}^*_\mathbf{r}(\Delta t)|^2\rangle}, \tag{68}$$

in terms of non-dimensional variables. Equation (68) is used for the calculation of the correction factor of the drag coefficient from the numerical data. This value will be compared to the analytical value given in [35], [36].

To calculate the drag coefficient from equation (68) the relative velocity of the sphere is required. This is calculated by the conservation of the total linear momentum

$$\rho^*_s\mathbf{U}^*\psi + \rho^*_f\mathbf{U}^*_f\left(1-\psi\right) = 0, \tag{69}$$

and

$$\mathbf{U_r}^* = \mathbf{U}^* - \mathbf{U}^*_f, \tag{70}$$

since, $\rho_s = \rho_f$

$$\mathbf{U_r}^* = \mathbf{U}^* - \mathbf{U}^* \frac{-\psi}{1-\psi} = \frac{\mathbf{U}^*}{1-\psi}, \tag{71}$$

where $\psi = \dfrac{\text{volume of particle}(V_P)}{\text{volume of complete domain}(V_\Omega)}$ is the volume fraction of the solid.

Hence,

$$\langle |\mathbf{U}_\mathbf{r}^*|^2 \rangle = \left(\frac{1}{1-\psi} \right)^2 \langle |\mathbf{U}^*|^2 \rangle. \tag{72}$$

The variance of the linear velocity of the solid is computed by an ensemble average

$$\langle |\mathbf{U}^*|^2 \rangle = \frac{1}{N_s - 1} \sum_{k=1}^{N_s} \left(\mathbf{U}_k^* - \overline{\mathbf{U}}^* \right)^2, \tag{73}$$

where

$$\overline{\mathbf{U}}^* = \frac{1}{N_s} \sum_{k=1}^{N_s} \mathbf{U}_k^*, \tag{74}$$

and N_s is the total number of realizations, which has to be understood in the same way as it has been already explained for the two-dimensional Brownian motion.

For the qualitative validation of the Brownian motion the probability density function (PDF) of the relative linear velocity of the sphere is shown and fitted with a Gaussian distribution. The x-component of the relative linear velocity is shown in figure 5. Within the accuracy limits of the numerical method, the PDF of the three velocity components are identical and show a very good agreement with the Gaussian distribution.

In figure 6, the histogram of the simulation data is compared with the Gaussian distribution of velocity with mean zero and variance $1/(\pi R^* \xi_{c_A})$, where ξ_{c_A} denotes the analytical value of the correction factor to the drag coefficient. Here a finer binning has been used for the histogram, which leads to stronger fluctuations in the coarse-grained data compared to figure 5.

The numerically computed value of the drag correction factor is computed from equation (68), which can be compared to the analytical value. In table 1 we do this comparison for different numbers of particles in the numerical scheme (on average over the complete simulation). The results shown in table 1 are for the same volume fraction of the solid, which is $\psi = 0.008$.

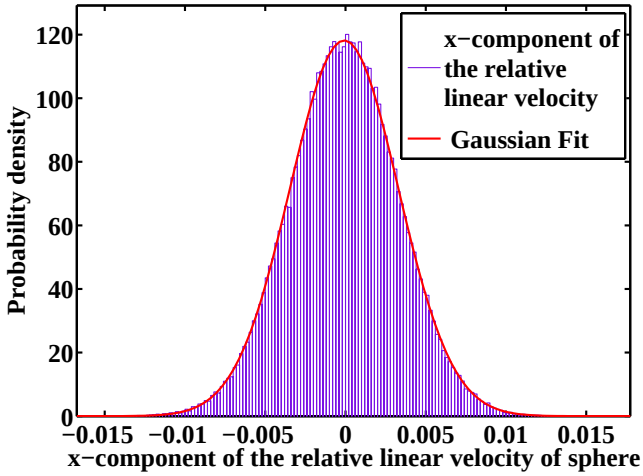

Figure 5: Gaussian fit to the PDF of the x-component of the relative linear velocity of the sphere.

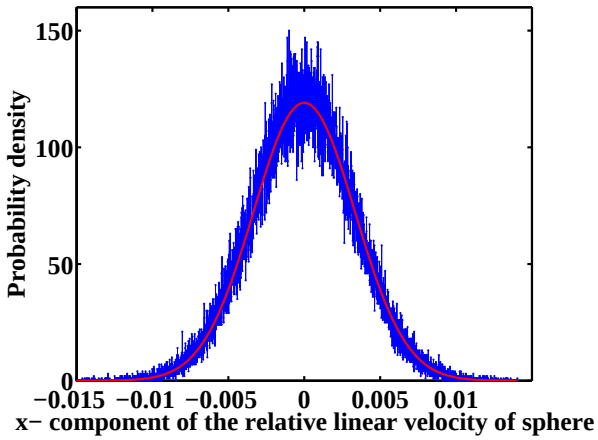

Figure 6: Numerically computed PDF of the relative linear velocity compared to the analytical result for diffusion in a spatially periodic domain.

We have also estimated the confidence interval for the numerical value of the drag correction factor with 95% confidence.

Consider an ensemble of N_s values of $\mathbf{U}_\mathbf{r}^*$ computed from N_s realizations. If $\mathbf{U}_\mathbf{r}^*$ obeys a Gaussian distribution of mean μ_{N_s} and variance $\sigma_{N_s}^2$ then the confidence interval for $\sigma_{N_s}^2$ is given by

$$\frac{(N_s-1)\langle|\mathbf{U}_\mathbf{r}^*|^2\rangle}{\chi^2_{\alpha/2,N_s-1}} < \sigma^2_{N_s} < \frac{(N_s-1)\langle|\mathbf{U}_\mathbf{r}^*|^2\rangle}{\chi^2_{1-\alpha/2,N_s-1}}, \tag{75}$$

with $100(1-\alpha)\%$ confidence. χ^2_{α,N_s-1} denotes the chi-square distribution with N_s-1 degrees of freedom, and α is defined by the probability density $f(\chi^2_{N_s-1})$ of $\chi^2_{N_s-1}$ as

$$1-\alpha = \int_0^{\chi^2_{\alpha,N_s-1}} f(\chi^2_{N_s-1})\,\mathrm{d}\chi^2_{N_s-1}. \tag{76}$$

The equations (75) and (68) give the confidence interval for ξ_c as

$$\frac{\chi^2_{1-\alpha/2,N_s-1}}{N_s-1}\xi_{c_s} < \xi_c < \frac{\chi^2_{\alpha/2,N_s-1}}{N_s-1}\xi_{c_s}, \tag{77}$$

where ξ_{c_s} denotes the numerical value of the drag correction factor for the considered ensemble. From table 1 one can observe a good agreement be-

M_a	Analytical Value	From Simulation	95% Confidence Interval	% Error
100700	1.525	1.4899	1.5084 - 1.4714	2.3
132350	1.525	1.5021	1.5207 - 1.4835	1.5
169371	1.525	1.4933	1.5118 - 1.4748	2.0

Table 1: Comparison of numerical and analytical values of the drag correction factor.

tween analytical and numerical values of the drag correction factor. This confirms that the numerics is able to reproduce the Stokes-Einstein relation and demonstrates the Brownian dynamics of a solid sphere immersed in an incompressible fluid by solving the fluctuating hydrodynamic equations.

5. Conclusions

In the present work, a meshfree discretization for a system comprising a fluctuating incompressible fluid and a suspended solid body has been presented and validated via an investigation of Brownian motion of the body.

No external forces on the solid structure other than the hydrodynamic force from the surrounding fluid have been considered. The LLNS equations for the fluctuating fluid have been coupled with the Newton-Euler equations for the motion of the body.

Qualitative and quantitative validations have been done for Brownian dynamics in two and three dimensions. In particular, the Stokes-Einstein relation is considered to calculate the corresponding correction factor for the drag coefficient in a three-dimensional spatially periodic system from the simulation data. The numerical value of the correction factor has been compared with the available analytical value, showing good agreement.

Moreover, a two-dimensional implementation of the fluid-structure system has been worked out. On a qualitative level, the Brownian motion of a disc was studied. Because of the Stokes' paradox, the quantitative validation for the two-dimensional case was done for a pure fluid system. The result shows good agreement with previous studies on the two-dimensional Stokes-Einstein relation for not too small values of the density.

The validation of Stokes-Einstein relation ensures the continuum fluctuation-dissipation theorem (FDT). It still needs to be verified at the discrete level. The numerical validation of the discrete FDT by static and dynamic structure factors is a future task of the authors. The study of fluid-fluid interfaces and the dynamics of small particles at these interfaces with fluctuating hydrodynamics in the framework of a meshfree discretization will be also the subject of future work.

Acknowledgment: This work was partially supported by the German Research Foundation (DFG), grant number KL 1105/20-1 and by the German Academic Exchange Service (DAAD) PhD program MIC.

References

[1] A. Vailati, R. Cerbino, S. Mazzoni, C. J. Takacs, D. S. Cannell, M. Giglio, Fractal fronts of diffusion in microgravity, Nature Communication 2 (2011) 290.

[2] A. Donev, J. B. Bell, A. de la Fuente, A. L. Garcia, Diffusive transport by thermal velocity fluctuations, Physical Review Letters 106 (2011) 204501.

[3] F. Detcheverry, L. Bocquet, Thermal fluctuations in nanofluidic transport, Physical Review Letters 109 (2012) 024501.

[4] J. M. O. D. Zárate, J. V. Sengers, Hydrodynamic Fluctuations in Fluids and Fluid Mixtures, Elsevier, The Netherlands, 2006.

[5] L. D. Landau, E. M. Lifshitz, Statistical Physics, Course of Theoretical Physics, volume 5, Pergamon press, New York, 1980.

[6] L. D. Landau, E. M. Lifshitz, Fluid mechanics, Course of Theoretical Physics, volume 6, Pergamon Press, London, 1959.

[7] P. Español, Stochastic differential equations for non-linear hydrodynamics, Physica A: Statistical Mechanics and its Applications 248 (1998) 77–96.

[8] A. L. Garcia, C. Penland, Fluctuating hydrodynamics and principal oscillation pattern analysis, Journal of Statistical Physics 64 (1991) 1121–1132.

[9] M. M. Mansour, A. L. Garcia, G. C. Lie, E. Clementi, Fluctuating hydrodynamics in a dilute gas, Physical Review Letters 58 (1987) 874–877.

[10] A. L. Garcia, M. M. Mansour, G. C. Lie, E. Clementi, Numerical integration of the fluctuating hydrodynamic equations, Journal of Statistical Physics 47 (1987) 209–228.

[11] J. B. Bell, A. L. Garcia, S. A. Williams, Numerical methods for the stochastic landau - lifshitz navier - stokes equations, Physical Review E 76 (2007) 016708.

[12] A. Donev, E. Vanden-Eijnden, A. Garcia, J. B. Bell, On the accuracy of explicit finite-volume schemes for fluctuating hydrodynamics, Communications in Applied Mathematics and Computational Science 5 (2010) 149–197.

[13] J. B. Bell, A. L. Garcia, S. Williams, Computational fluctuating fluid dynamics, ESAIM: Mathematical Modelling and Numerical Analysis 44 (2010) 1085–1105.

[14] F. B. Usabiaga, J. B. Bell, R. Delgado-Buscalioni, A. Donev, T. G. Fai, B. E. Griffith, C. S. Peskin, Staggered schemes for fluctuating hydrodynamics, SIAM Journal of Multiscale Modeling and Simulation 10 (2012) 1369–1408.

[15] A. Pandey, A. Klar, S. Tiwari, Meshfree method for fluctuating hydrodynamics, Mathematics and Computers in Simulation 82 (2012) 2157–2166.

[16] N. Sharma, N. A. Patankar, Direct numerical simulation of the brownian motion of particles by using fluctuating hydrodynamics equations, Journal of Computational Physics 201 (2004) 466–486.

[17] P. J. Atzberger, Stochastic eulerian lagrangian methods for fluid-structure interactions with thermal fluctuations, Journal of Computational Physics 230 (2011) 2821–2837.

[18] P. E. nol, M. Revenga, Smoothed dissipative particle dynamics, Physical Review E 67 (2003) 1–12.

[19] G. R. Liu, M. Liu, Smoothed Particle Hydrodynamics, a meshfree particle method, World Scientific Publishing Co. Pte. Ltd., Singapore, 2003.

[20] E. G. Flekkøy, P. V. Coveney, G. De Fabritiis, Foundations of dissipative particle dynamics, Physical Review E 62 (2000) 2140–2157.

[21] A. Debussche, J. Printrms, Weak order for the discretization of the stochastic heat equation, Mathematics of computation 78 (2009) 845–863.

[22] A. Jentzen, P. E. Kloeden, The numerical approximation of stochastic partial differential equations, Milan journal of Mathematics 77 (2009) 205–244.

[23] G. D. Prato, Kolmogorov equations for stochastic PDEs, Birkhäuser, Basel, 2004.

[24] A. J. Chorin, Numerical solution of the navier-stokes equations, Mathematics of Computation 22 (1968) 745–762.

[25] H. H. Hu, D. D. Joseph, M. J. Crochet, Direct simulation of fluid particle motions, Theoretical and Computational Fluid Dynamics 3 (1992) 285–306.

[26] H. H. Hu, N. A. Patankar, M. Y. Zhu, Direct numerical simulations of fluid-solid systems using Arbitrary-Lagrangian-Eulerian technique, Journal of Computational Physics 169 (2001) 427–462.

[27] R. Glowinski, T. Pan, T. I. Hesla, D. D. Joseph, A fictitious domain approach to the direct numerical simulation of incompressible viscous flow past moving rigid bodies: Application to particulate flow, Journal of Computational Physics 169 (2001) 363–426.

[28] S. Tiwari, J. Kuhnert, Finite pointset method based on the projection method for simulations of the incompressible Navier-Stokes equations, Lecture Notes in Computational Science and Engineering 26 (2002) 373–387.

[29] S. Tiwari, J. Kuhnert, Grid free method for solving Poisson equation, Wavelet Analysis and Applications, New Age International Publishers (2004) 151–166.

[30] J. C. Lewis, On the Einstein-Stokes diffusion coefficient for Brownian motion in two dimensions, Physics Letters A 44A (1973) 245–246.

[31] T. Keyes, I. Oppenheim, Bilinear hydrodynamics and the Stokes-Einstein law, Physical Review A 8 (1973) 937–949.

[32] R. G. Rojo, S. Luding, J. J. Brey, Transport coefficients for dense hard-disk systems, Physical Review E 74 (2006) 1–11.

[33] B. Liu, J. Goree, Test of the Stokes-Einstein relation in a two-dimensional Yukawa liquid, Physical Review Letters 96 (2006) 1–4.

[34] R. Srivastava, K. N. Khanna, Stokes-Einstein relation in two and three-dimensional fluids, Journal of Chemical Engineering Data 54 (2009) 1452–1456.

[35] H. Hasimoto, On the periodic fundamental solution of the Stokes equations and their application to viscous flow past a cubic array of spheres, Journal of Fluid Mechanics 5 (1959) 317–328.

[36] A. A. Zick, G. M. Homsy, Stokes flow through periodic arrays of spheres, Journal of Fluid Mechanics 115 (1982) 13–26.